Nature. Author manuscript; available in PMC 2017 February 18.

Published in final edited form as:
Nature. 2016 August 18; 536(7616): 344–348. doi:10.1038/nature18958.

Asymmetric division of contractile domains couples cell positioning and fate specification

Jean-Léon Maître[1,2,3], **Hervé Turlier**[#1], **Rukshala Illukkumbura**[#1], **Björn Eismann**[1,5], **Ritsuya Niwayama**[1], **François Nédélec**[1], and **Takashi Hiiragi**[1,3]

[1]European Molecular Biology Laboratory, Meyerhofstrasse 1, 69117 Heidelberg, Germany

[#] These authors contributed equally to this work.

Abstract

During pre-implantation development, the mammalian embryo self-organizes into the blastocyst consisting of an epithelial layer encapsulating the inner-cell mass (ICM), which gives rise to all embryonic tissues1. In mice, oriented cell division, apico-basal polarity and acto-myosin contractility are thought to contribute to the formation of the ICM2–5. However, how these processes work in concert remains unclear. Here, we show that asymmetric segregation of the apical domain generates blastomeres with different contractility, which triggers their sorting into inner and outer positions. 3D physical modeling of embryo morphogenesis reveals that cells internalize only when differences in surface contractility exceed a predictable threshold. We validate this prediction using biophysical measurements and successfully re-direct cell sorting within the developing blastocyst using maternal myosin (*Myh9*) knockout chimeric embryos. Finally, we find that loss of contractility causes blastomeres to show ICM-like markers regardless of their position. In particular, contractility controls Yap sub-cellular localization6, raising the possibility that mechanosensing occurs during blastocyst lineage specification. We conclude that contractility couples the positioning and fate specification of blastomeres. We propose that this ensures the robust self-organization of blastomeres into the blastocyst, which confers remarkable regulative capacities to mammalian embryos.

During the 8- to 16-cell stage transition, oriented divisions can push one of the daughter cells towards the inside of the embryo5,7,8. Alternatively, blastomeres were observed to internalize after the 8- to 16-cell stage division, possibly driven by differences in cell

[3]Correspondence and requests for materials should be addressed to J-L.M. (jean-leon.maitre@curie.fr) or T.H. (hiiragi@embl.de).
[2]Present address: Mechanics of Mammalian Development Group, Institut Curie, CNRS UMR 3215, INSERM U934, 26, rue d'Ulm, 75248 Paris Cedex 05, France
[5]Present address: Bioquant, Im Neuenheimer Feld 267, 69120 Heidelberg, Germany

Author contributions

J-L.M. designed the project and experiments, and wrote the manuscript with input from all authors. J-L.M. and B.E. performed and analyzed the tension and lineage mapping experiments. J-L.M. and R.I. performed and analyzed the remaining experiments. R.N. helped with image analysis of the periodic contractions. H.T. designed the physical model and performed the simulations with help from F.N.. T.H. supervised the study and helped designing the project.

Author information

The authors declare no competing financial interests.

Europe PMC Funders Author Manuscripts

contractility2,3. How the embryo generates cell populations with distinct contractile properties is however unknown, and the physical mechanism by which this leads to internalization remains disputed2,3.

We first investigate the origin of the differences in contractility among blastomeres at the 16-cell stage. During the 8-cell stage, blastomeres polarize by forming an apical domain, which occupies only a portion of the contact-free surface. This apical material can be asymmetrically inherited during the following division2,9, giving rise to both polarized and unpolarized blastomeres within the 16-cell stage embryo, as can be observed from the levels of the essential apical protein aPKC4,10,11 (Extended Data Fig. 1). We observe that unpolarized blastomeres, with low levels of aPKC, show higher cortical levels of myosin than polarized ones (Extended Data Fig. 1). Moreover, in embryos knocked-out for two isoforms of aPKC4,10, we observe no reduction of myosin levels where the apical domain would normally be, suggesting that aPKC antagonizes cortical myosin accumulations at the apical domain (Extended Data Fig. 1). As a consequence of reduced levels of myosin, one expects the apical domain to exhibit reduced contractility. To test this, we take advantage of the periodic contractions that appear during the 8-cell stage12,13 and use them as a proxy of contractility. Upon polarization of 8-cell stage blastomeres, we measure contractions of lower amplitude at the apical domain than in the rest of the cortex (apical/non-apical: 59 ± 23%, Mean ± SD, n = 17 blastomeres, Fig. 1a-e, Supplementary Video 1). After asymmetric division of 8-cell stage blastomeres, the polarized 16-cell stage blastomeres often show no detectable periodicity (52% of 23 polarized blastomeres showing contractions, Fig. 1d, Supplementary Video 2) and their contractions display lower amplitudes than those of unpolarized blastomeres (polarized/unpolarized: 65 ± 26%, Mean ± SD, n = 23 doublets, Fig. 1f-i). More precisely, we find that this difference in contractility between polarized and unpolarized blastomeres intensifies as cells internalize (Extended Data Fig. 2). Contractility in polarized blastomeres remains dampened by the apical domain (Fig. 1j, Extended Data Fig. 1-2) and polarized sister cells resulting from symmetric divisions show little cortical heterogeneity and do not internalize (Extended Data Fig. 2). On the contrary, unpolarized blastomeres increase their contractility, as initiated during compaction at the 8-cell stage12, resulting in increasing heterogeneity in doublets stemming from asymmetric divisions (Fig. 1j, Extended Data Fig. 2). In summary, we identify the asymmetric inheritance of the apical domain during the 8- to 16-cell stage division as the source of differences in contractility among blastomeres.

How these differences in cell contractility physically translate into the internalization of the ICM remains unclear2,3. To quantitatively describe the mechanism of internalization, we consider the blastomeres surface tensions, which are controlled by acto-myosin contractility14, and build thereupon a physical model of their configuration. At first, we consider a cell doublet as a minimal system in which one cell envelops its neighbor in an entosis-like process15 (Extended Data Fig. 2, Supplementary Video 5). This reductionist approach is justified by the fact that doublets resulting from asymmetrically divided 8-cell stage blastomeres recapitulate both the morphogenesis and fate specification of the whole embryo16,17. Noting γ_c the surface tension at cell-cell contacts and γ_i the tension at the cell-medium interface of the cell i (with $i = 1$ or 2 for a cell doublet, Fig. 2a), we define three dimensionless parameters: a compaction parameter $\alpha = \gamma_c / 2\gamma_2$; a volume asymmetry $\beta =$

$(V_1 / V_2)^{1/3}$, where V_1 and V_2 are the volumes of each cell; and a tension asymmetry $\delta = \gamma_1 / \gamma_2$. We can analytically derive the conditions for cell internalization (Fig. 2b-c, Supplementary Video 3, Supplementary Note). Full internalization occurs whenever $\delta > 1 + 2\alpha$ (Fig. 2b-c), thus defining an internalization threshold $\delta_c = 1 + 2\alpha$ for the tension asymmetry, in agreement with previous numerical studies18–20. Before this transition, partial internalization configurations are predicted, which match the configurations observed experimentally in doublets of 16-cell stage blastomeres (Extended Data Fig. 2, Supplementary Video 5). Interestingly, the internalization threshold δ_c is not influenced by the size asymmetry β but depends critically on the compaction parameter α (Extended Data Fig. 3). Modulating α in the absence of tension asymmetry is however not sufficient for driving internalization. For the value of the compaction parameter measured at late 8-cell stage12, $\alpha \sim 0.25$, we predict that any tension asymmetry δ higher than $\delta_c \sim 1.5$, should lead to complete internalization (Fig. 2b-c). Therefore, when measuring tension asymmetries, we expect that δ should not exceed ~ 1.5, otherwise the cell should be fully internalized and hence inaccessible to non-invasive methods.

To generalize this approach to the formation of the ICM in an embryo with 16 cells, we build a 3D numerical model of the embryo, using a multi-material mesh-based surface-tracking method21 (Supplementary Note). We find in simulated embryos the same internalization conditions as in cell doublets, with a transition occurring above the threshold value $\delta_c \sim 1.5$ (Fig. 2d, Extended data Fig. 7, Supplementary Video 4). Therefore, the same physical mechanisms can explain the envelopment of one cell by another15 and the sorting of cells within a tissue18,19,22,23.

To experimentally test the predictions of the model, we use microaspiration to measure the surface tensions of sister cells after the 8- to 16-cell stage division, visualize their internalization and then track their position within the blastocyst (Fig. 3a, Supplementary Video 6). Sister cells remaining at the surface of the embryo and failing to contribute to the ICM in the blastocyst show no tension asymmetry at the 16-cell stage ($\delta = 1.04 \pm 0.03$, Mean ± SD, n = 8 pairs of sister cells, Fig. 3b). On the other hand, when one sister cell internalizes after the 8- to 16-cell stage division and contributes to the ICM within the blastocyst, we measure a tension asymmetry of 1.24 ± 0.17 (Mean ± SD, n = 7 pairs of sister cells, Fig. 3b). This confirms that asymmetric divisions are the source of tension heterogeneities in the embryo. Furthermore, the observation that internalizing cells are the only ones showing tension heterogeneity relative to their sister cells supports the hypothesis that tension heterogeneity is sufficient to drive cell internalization. Finally, the measured tension asymmetries are indeed lower than the internalization threshold value $\delta_c \sim 1.5$, as predicted by our theory.

To directly test the proposed internalization mechanism, we first generate embryos that lack the maternal allele of *Myh9*24 (mMyh9 hereafter), the specific isoform of myosin heavy chain that is required for pre-implantation development (zygotic25 and maternal zygotic Myh10 knockout embryos form normal blastocyst, Supplementary Video 7). Although compaction is delayed due to their inability to generate sufficient tensions12 (Extended Data Fig. 4), those embryos form blastocysts (Supplementary Video 8) and viable offspring. Then, we transplant onto a mMyh9 host embryo a WT blastomere, which typically

internalizes (60% of 20 grafted blastomeres internalized, Fig. 3d, h, Supplementary Video 9, corresponding numerical simulation Fig. 3e, Supplementary Video 10) and contributes to the ICM of the host embryo. In contrast, when transplanted onto WT embryos, a mMyh9 blastomere always remains at the surface of the embryo (none of 12 grafted blastomeres internalized, Fig. 3e, h, Supplementary Video 11 corresponding numerical simulation Fig. 3g, Supplementary Video 12), and stretches to envelop blastomeres of the host embryo. In comparison, transplanting WT cells onto WT hosts leads to a lower internalization frequency than with mMyh9 hosts (31% of 33 blastomeres internalized, $p = 0.05$, Fig. 3c, h, Supplementary Video 13). We conclude that the hierarchy of contractility between blastomeres is sufficient to direct cell internalization. As internalizing cells do not have an apical domain (Fig. 1, Extended Data Fig. 1-2) and do not require intact contractility of neighboring cells (Fig. 3d), the mechanism by which cells internalize is analogous to a cell sorting process22 and is distinct from an apical constriction, as previously proposed3.

While cells adopt their position within the embryo, they segregate into two distinct lineages: trophectoderm and ICM. In the mouse embryo, this lineage specification is regulated by Yap sub-cellular localization4,11, which, in cultured cells, is regulated by contractile forces6. Therefore, we test if contractility influences Yap localization and thereby fate specification. In agreement with previous studies2,4, we find less cytoplasmic phosphorylated Yap in cells closer to the surface than in the internalized ones (Extended Data Fig. 5a, h). These blastomeres initiate trophectoderm specification as surface cells show highest Cdx2 levels (Extended Data Fig. 5a, o). In embryos treated with different concentrations of the myosin inhibitor Blebbistatin (Bb), the correlation between these fate markers and cell position is weakened in a dose-dependent manner (Extended Data Fig. 5-6). Moreover, mMyh9 embryos show similar defects at the 16-cell stage (Extended Data Fig. 5g, n, u, 6c, f), despite being viable (unlike Bb-treated embryos). While inhibiting contractility de-compacts embryos12, the position of cells is not shuffled, and yet the localization of Yap is affected. During cell internalization, outer cells deform extensively. This is especially the case for doublets in which, similarly to complete embryos, cytoplasmic localization of phosphorylated Yap is lowest for outer cells (Fig. 4a, c, d). When cell deformation is blocked by Bb treatment, phosphorylated Yap localization and Cdx2 levels become homogeneous within doublets (Fig. 4b-f). Remarkably, inhibition of contractility causes both blastomeres to become inner cell-like with respect to phosphorylated Yap localization and Cdx2 levels, despite their external position (Fig. 4). This is consistent with internalizing cells reducing their contractility over their entire surface, since cell-cell contacts have a contractility equivalent to Bb-treated cells12. Together, these results indicate that without contractile forces, blastomeres adopt an inner cell-like fate, regardless of their position. Therefore, disrupting contractility uncouples morphogenesis and fate specification. Moreover, the control of Yap sub-cellular localization by contractile forces, reminiscent of those from cell culture studies6, raises the possibility that lineage specification in the blastocyst could be mechanosensitive. Whether cells may sense their macroscopic deformation26 or stresses at the molecular level27, will require further studies. Such mechanosensitivity could explain why inner cell-like localization of Yap is often observed for blastomeres before they have completed their internalization2,4 (Extended Data Fig. 5-6). We propose that the coupling of cell positioning and fate specification by contractility

enables blastomeres to anticipate their final position and initiate their differentiation accordingly.

Apico-basal polarity can control the position of blastomeres by orienting the 8- to 16-cell stage divisions relative to the surface of the embryo5. However, oriented cell divisions do not guarantee that internalized cells will be maintained inside the embryo. We find that apico-basal polarity also controls internalization by maintaining low contractility at the apical domain (Fig. 1). This allows unpolarized blastomeres to outcompete their polarized neighbors when their contractility grows above a threshold value (Fig. 2-3). The resulting cell sorting is a fail-safe mechanism to one-shot oriented cell divisions. Such complementary mechanisms, together with the ability of cells to read mechanical cues6 to guide their differentiation28 (Fig. 4), can account for the regulative capacity of early mammalian embryos7. From this study, a self-organization framework determining the initial steps of morphogenesis and lineage specification in mammalian embryos is emerging.

Methods

Embryo work

Recovery and culture—All animal work is performed in the animal facility at the European Molecular Biology Laboratory, with permission by the institutional veterinarian overseeing the operation (ARC number TH11 00 11). The animal facilities are operated according to international animal welfare rules (Federation for Laboratory Animal Science Associations guidelines and recommendations).

Embryos are isolated from superovulated female mice mated with male mice. Superovulation of female mice is induced by intraperitoneal injection of 5 international units (IU) pregnant mare's serum gonadotropin (PMSG, Intervet Intergonan), followed by intraperitoneal injection of 5 IU human chorionic gonadotropin (hCG, Intervet Ovogest 1500) 44-48 hours later. Two-cell-stage (embryonic day 1.5; E1.5) embryos are recovered by flushing oviducts from plugged females with 37°C FHM (Millipore, MR-024-D) using a custom-made syringe (Acufirm, 1400 LL 23).

Embryos are handled using an aspirator tube (Sigma, A5177-5EA) equipped with a glass pipette pulled from glass micropipettes (Blaubrand intraMark).

Embryos are placed in KSOM (Millipore, MR-121-D) or FHM supplemented with 0.1% BSA (Sigma, A3311) in 10 μL droplets covered in mineral oil (Sigma, M8410 or Acros Organics). Embryos are cultured in an incubator with a humidified atmosphere supplemented with 5% CO_2 at 37°C.

For imaging, embryos are placed in 5 cm glass-bottom dishes (MatTek).

Mouse lines—(C57BL/6xC3H) F1 hybrid strain is used for wild-type (WT).

To visualize filamentous actin, LifeAct-GFP mice (Tg(CAG-EGFP)#Rows) are used29. To visualize plasma membranes, mTmG mice (Gt(ROSA)26Sor$^{tm4(ACTB-tdTomato,-EGFP)Luo}$) are used30. To visualize nuclei, H2B-GFP mice are used 31. Genes are deleted maternally using

Zp3-cre (Tg(Zp3-cre)93Knw) mice32. To generate mMyh9 embryos, $Myh9^{tm5RSad}$ mice are used24 to breed $Myh9^{tm5RSad/tm5RSad}$; $Zp3^{Cre/+}$ mothers with WT fathers. To generate mzMyh10 embryos, $Myh10^{tm7Rsad}$ mice were used33 to breed $Myh10^{tm7Rsad/tm7Rsad}$; $Zp3^{Cre/+}$ mothers with $Myh10^{+/-}$ fathers. To generate aPKC KO embryos, $Prkci^{tm1Kido}$ 10 and $Prkcz^{tm1.1Cda}$ 4 mice are used to breed $Prkci^{-/-}$; $Prkcz^{+/-}$ fathers with Prkci-/- ; $Prkcz^{tm1.1Cda/+}$; $Zp3^{Cre/+}$ mothers.

Mice were used from 6 weeks old on.

Chemical reagents—Blebbistatin (+), an inactive enantiomere of the inhibitor, or (-), the selective inhibitor of myosin II ATPase activity, (Tocris, 1853 and 1852) 50 mM DMSO stocks are diluted to 5, 12.5 or 25 μM in KSOM.

Isolation of blastomeres at the 8- and 16-cell stage—Embryos are dissected out of their *zona pellucida* (ZP) at the 2- to 4-cells stage. ZP-free 8- or 16-cell stage embryos are placed into Ca^{2+}-free KSOM for 5-10 min before being aspirated multiple times (typically between 3-5 times) through a narrow glass pipette (with a radius between that of an 8- or 16-cell stage blastomere and of the whole embryo) until dissociation of cells. To form doublets of polarized and unpolarized 16-cell stage blastomeres, an 8-cell stage blastomere is cultured until asymmetric division. To form chimaeras, 16-cell stage blastomeres are grafted onto a complete embryo using a mouth pipette.

Immunostaining—Primary antibody targeting the double phosphorylated form (Thr18/Ser19) of the myosin regulatory light-chain (Cell Signaling, 3674), PKC-ζ (Santa Cruz, sc-17781), Yap (Abnova, M01, clone 2F12) or its Ser127 phosphorylated form (Cell Signaling, 4911) are used at 1:100. The primary antibody targeting Cdx2 (Biogenex, MU392A-UC) or phosphorylated form (Ser1943) of the non-muscle myosin heavy chain Myh9 (Cell Signaling, 5026) are used at 1:200.

Secondary antibody targeting mouse or rabbit IgG coupled to Alexa Fluor 488 or 546 (Life Technologies) are used at 1:250. Alexa Fluor 633-coupled (ThermoFisher, A22284) phalloidin is used at 1:250.

Micropipette aspiration—As described previously12, a microforged micropipette coupled to a microfluidic pump (Fluigent, MFCS) is used to measure the surface tension of cells. In brief, micropipettes of radii 7-8 μm for 8-cell stage embryos and 2.5-3.5 μm for 16-cell stage embryos are usd to apply step-wise increasing pressures on blastomeres until reaching a deformation which has the radius of the micropipette (R_p). At steady-state, the surface tension γ_1 of the blastomere is calculated based on Young-Laplace's law: $\gamma_1 = P_c / 2 (1/R_p - 1/R_c)$, where P_c is the pressure used to deform the cell of radius R_c.

Asymmetric division tracing—To measure the tension of sister cells at the 16-cell stage, time-lapse images of mTmG and H2B-GFP expressing embryos were taken every 30 min from the 8-cell stage onwards. The 8- to 16-cell stage divisions are tracked, the time-lapse is paused in order to measure the surface tension of both sister cells. After resuming the time-lapse, the measured cells are tracked until blastocyst stage. When both sister cells remain at

the surface of the embryo, the division is considered symmetric, whereas when one sister cell internalizes during the 16-cell stage and becomes part of the ICM, the division is considered asymmetric.

Microscopy—Tension measurements are performed on a Zeiss Axio Observer microscope with a dry 20x/0.8 PL Apo DICII objective. The microscope is equipped with an incubation chamber to keep the sample at 37°C. Confocal images are taken using an inverted Zeiss Observer Z1 microscope with a CSU-X1M 5000 spinning disc unit. Excitation is achieved using 488 nm, 561 nm and 633 nm laser lines through a 63x/1.2 C Apo W DIC III water immersion objective. Emission is collected through 525/50 nm, 605/40 nm, 629/62 nm band pass or 640 nm low pass filters onto an EMCCD Evolve 512 camera. The microscope is equipped with an incubation chamber to keep the sample at 37°C and supply the atmosphere with 5% CO_2.

Data analysis

Shape analysis—Using FIJI, we manually fit a circle onto the cell-medium interface to measure the radius of curvature of the cell R_c. We use the angle tool to measure the contact angles θ_1, θ_2 and θ_c. We draw a line perpendicular to the micropipette tip and use the linescan function to measure the diameter of the micropipette and calculate R_p.

Intensity ratio measurements—Using FIJI, we pick confocal slices cutting through the equatorial plane of the apical domain or of two contacting cells. We draw a ~1 μm thick line along the cell-medium interface of the apical and non-apical regions or of each cell and measure the mean intensity. The apical region is defined by visually observing aPKC or mTmG enrichment in the central region of the cell-medium interface. For aPKC KO embryos, the actin-rich region at the center of the cell-medium interface is selected. The transition zones between apical and non-apical or close to cell-cell contacts between polarized and unpolarized cells are excluded to calculate intensity ratios (~5 μm).

Using FIJI, we pick confocal slices cutting through the equatorial plane of the nucleus of a cell. We draw a 2.5 μm radius circle and measure the average intensity in the nucleus and, next to it, in the cytoplasm. We then calculate the nucleus to cytoplasm intensity ratio. For whole embryos, the closest distance of the nucleus to the surface of the embryo, marked by phalloidin staining, is measured using the line tool.

Periodic contractions analysis—To analyze periodic contractions, we used a previously described pipeline12. In brief, mTmG images are used to segments the cells outlines into 100 equidistant nodes for 8-cell stage blastomeres and 150 for 16-cell stage blastomeres doublets. From those nodes, three nodes spaced by 10 or 7 nodes (respectively for 8-cell stage blastomeres and 16-cell stage blastomeres doublets) are then taken to fit a circle and compute the local curvature from the inverse radius of this circle. Taking the local curvatures along the cell perimeter over time, a kymograph of local curvature is created. Applying a Fourier transform on the curvature changes over time at each node, we obtain the amplitude of nodes that are classified either as apical or non-apical, based on the mTmG signal that is enriched on the apical domain excluding about 10 nodes around the transition

between apical to non-apical domains. For doublets, nodes are classified either as inner or outer cell, based on, when applicable, the asymmetry of the internal contact angles (the cell with the largest internal contact angle being designated as the inner cell for ratio calculation) and/or, when applicable, by the asymmetry in cell size (the smallest cell being designated as the inner cell for ratio calculation). About 10 nodes near the contact edges are excluded from the analysis.

Code availability—Codes are available upon request.

Statistics—Mean, standard deviation, correlation coefficient, two-tailed Student's *t*-test and single-tailed Mann-Whitney *U*-test *p* values are calculated using Excel (Microsoft). Statistical significance of correlation coefficients is obtained from the Pearson correlation table.

The sample size was not predetermined and simply results from the repetition of experiments. No sample was excluded. No randomization method was used. The investigators were not blinded during experiments.

Europe PMC Funders Author Manuscripts

Europe PMC Funders Author Manuscripts

Extended Data

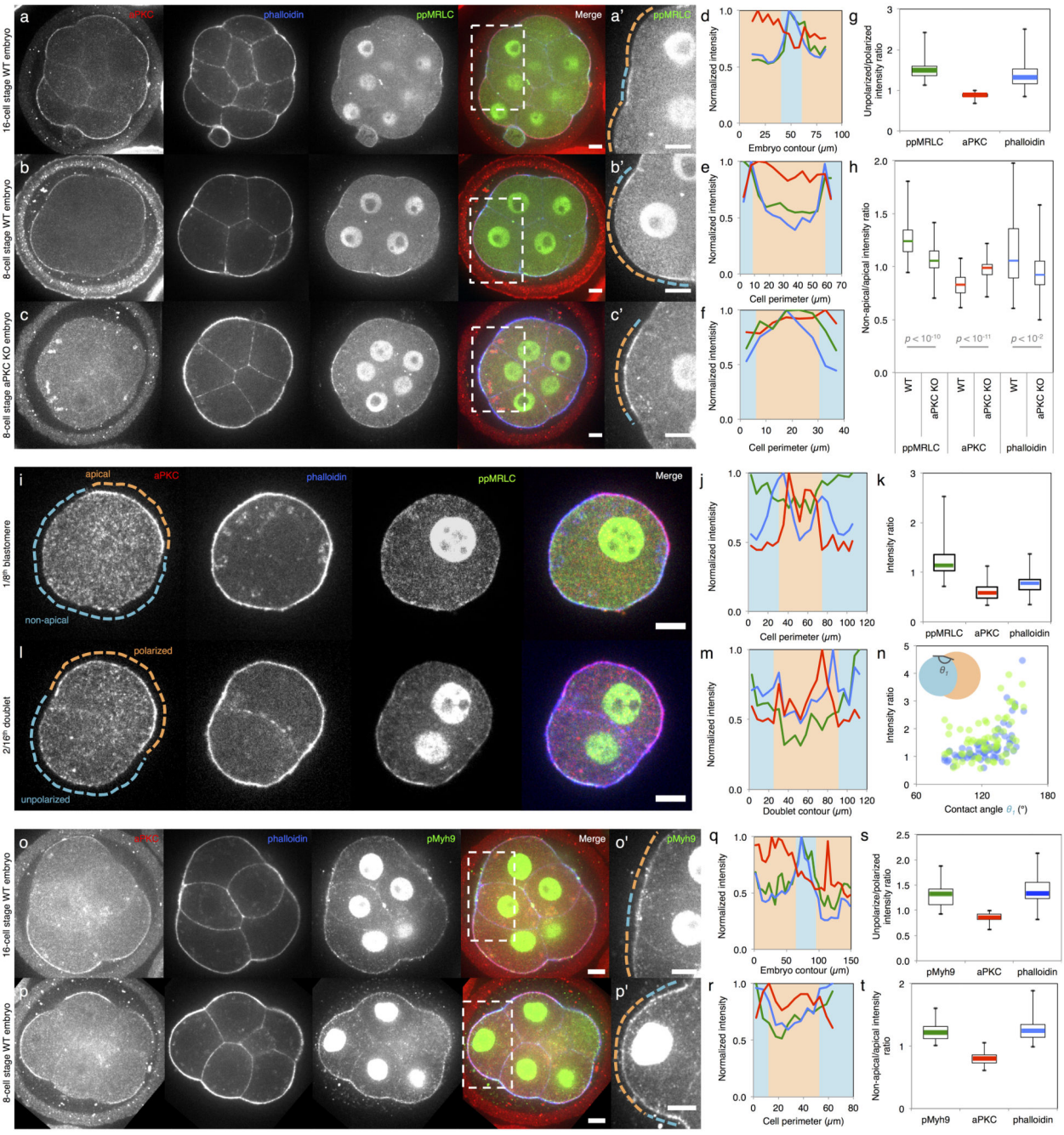

Extended Data Figure 1. aPKC antagonizes myosin phosphorylation at the apical domain

(a-c) Immunostaining of 16- (a) and 8-cell stage wild-type (b) and aPKC KO (c) embryos showing aPKC (red), phalloidin (blue) and ppMRLC (green, bi-phosphorylated Myosin Regulatory Light Chain). Enlarged images of ppMRLC are shown in a'-c'.

(d-f) Cortical intensity profiles under the dotted lines in a'-c'. Apical domains highlighted in orange and non-apical regions in blue.

(g-h) Boxplot of unpolarized/polarized blastomere intensity ratio at the 16-cell stage (43 neighbouring blastomeres from 35 embryos from 3 experiments) and non-apical/apical intensity ratio at the 8-cell stage for WT and aPKC KO embryos (68 and 58 blastomeres from 22 and 12 embryos from 2 and 3 experiments respectively). ppMRLC in green, aPKC in red and phalloidin in blue. Student *t* test *p* values between WT and aPKC KO.

At the 16-cell stage (a, d, g), blastomeres showing accumulations of ppMRLC and phalloidin at their cell-medium interfaces have less aPKC. At the 8-cell stage, the apical domain does not occupy the entirety of the cell-medium interface (b, e). The aPKC-rich apical domain shows less myosin than the aPKC-poor region of the cortex (b, e, h). In aPKC KO embryos (c, f, h), no aPKC-rich, nor ppMRLC-poor regions can observed at the cell-medium interface of blastomeres.

(i) Immunostaining of 8-cell stage blastomeres showing aPKC (red), phalloidin (blue), ppMRLC (green) and merged staining. The apical domain is highlighted in orange, the non-apical cortex in blue. Scale bar 10 μm.

(j) Intensity profile along the cell perimeter showing aPKC (red), phalloidin (blue) and ppMRLC (green). The apical intensity is highlighted in orange the non-apical cortex in blue.

(k) Box plot of apical and non-apical intensity ratio of cortical aPKC (red), phalloidin (blue) and ppMRLC (green) for 27 blastomeres from 3 experiments.

Blastomeres isolated at the 8-cell stage show an aPKC-rich region (i-k), which has less cortical ppMRLC and phalloidin than the aPKC-poor region of the cell-medium interface. The ppMRLC- and actin-rich regions are distinct from the baso-lateral domain of cells (their cell-cell contact), which have less ppMRLC and actin (a, b, c, l)12. This ppMRLC cortical region is therefore labeled “non-apical”.

(l) Immunostaining of doublets of 16-cell stage blastomeres showing aPKC (red), phalloidin (blue), ppMRLC (green) and merged staining. The polarized blastomere is highlighted in orange, the unpolarized one in blue. Scale bar 10 μm.

(m) Intensity profile along the doublet perimeter showing aPKC (red), phalloidin (blue) and ppMRLC (green). The polarized blastomere is highlighted in orange, the unpolarized one in blue.

Blastomeres isolated at the 8-cell stage divide to give rise to doublets of 16-cell stage blastomeres2,16. The polarized sister cell shows high aPKC and low ppMRCL/phalloidin at their cell-medium interfaces when compared to the non-polarized sister cell (l, m).

(n) Cortical intensity ratio of ppMRLC (green) and phalloidin (blue) between the inner and outer cells as a function of the inner contact angles θ_1 (Pearson R = 0.464 and 0.614, n = 67 doublets from 2 experiments, $p < 0.001$).

During the 16-cell stage, polarized blastomeres can envelop their unpolarized sister blastomeres (Supplementary Video 5)2,16. As envelopment occurs, the internal contact angles change (Extended Data Fig. 2). As the internal contact angles change, the asymmetry in cortical ppMRLC and phalloidin between sister blastomeres changes. After another division, a cyst consisting of 4 blastomeres forms (Supplementary Video 5). This structure is equivalent to the blastocyst in terms of gene expression16 (Figure 4).

(o-p) Immunostaining of 16- (o) and 8-cell stage (p) embryos showing aPKC (red), phalloidin (blue) and pMyh9 (green, Myosin heavy chain phosphorylated on S1943). Enlarged images of ppMRLC are shown in o’-p’.

(q-r) Cortical intensity profiles under the dotted lines in o'-p'. Apical domains highlighted in orange and non-apical regions in blue.
(s-t) Boxplot of unpolarized/polarized blastomere intensity ratio at the 16-cell stage (24 neighbouring blastomeres from 16 embryos from 3 experiments) and non-apical/apical intensity ratio at the 8-cell stage (34 blastomeres from 10 embryos from 3 experiments). pMyh9 in green, aPKC in red and phalloidin in blue.

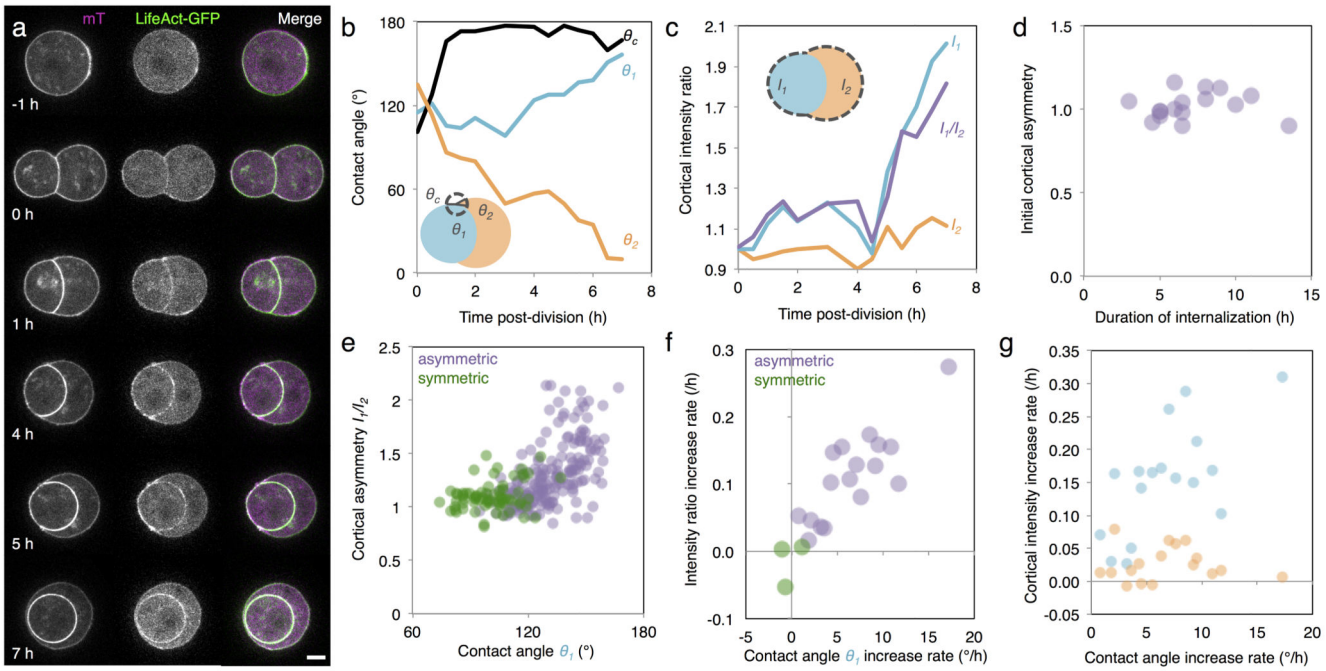

Extended Data Figure 2. Cortical asymmetries intensify during the 16-cell stage

(a) Time-lapse of mTmG (magenta) and LifeAct-GFP (green) expressing doublets of 16-cell stage blastomeres. Scale bar 10 μm.
(b-c) External (θ_c), and internal (θ_1 and θ_2) contact angles (b) and cortical LifeAct-GFP intensities of unpolarized I_1 and polarized I_2 blastomeres and intensity ratio I_1/I_2 (c) over time for the doublet shown in (a).
Blastomeres isolated at the 8-cell stage can divide asymmetrically to give rise to a polarized blastomere that will envelop its unpolarized sister blastomere (a). The external contact angle θ_c shows a rapid re-compaction of the cell doublet after division (b). The internal contact angles θ_1 and θ_2 indicate the progression of the envelopment process (b). As this happens, the cortical intensity of LifeAct-GFP of the internalizing blastomere I_1 increases while the one of the enveloping blastomere I_2 remains comparably more stable (c). This increases the cortical asymmetry I_1/I_2 (c).
(d) Initial cortical asymmetry over internalization time of doublets of 16-cell stage blastomeres (Pearson R = 0.064, n = 16 doublets from 4 experiments $p > 0.1$). The initial cortical asymmetry, calculated within 30 min after division, is 1.0 ± 0.1 (Mean ± SD, n = 17 doublets from 4 experiments) and does not control the time it takes for envelopment to occur (d).

(e) Intensity ratio as a function of the contact angle θ_1 of doublets throughout the 16-cell stage blastomeres (Pearson R = 0.573, 186 measurements on 17 asymmetric doublets (purple), p < 0.001 and Pearson R = 0.266, 69 measurements on 3 symmetric (green) doublets, $p < 0.1$, from 4 experiments).
As the internal contact angles change, the asymmetry in cortical LifeAct-GFP between sister blastomeres with distinct polarity changes.
(f) Cortical intensity ratio increase rate as a function of the contact angle θ_1 increase rate (Pearson R = 0.824, n = 17 asymmetric (purple), $p < 0.001$, and Pearson R = 0.393, n = 3 symmetric (green) doublets, $p > 0.1$, from 4 experiments).
(g) Cortical intensity increase rate as a function of the contact angle increase rate for the polarized (orange, Pearson R = -0.026, n = 17 asymmetric doublets, $p > 0.1$) and unpolarized blastomere (blue, Pearson R = 0.658, n = 17 asymmetric doublets, $p < 0.01$) of a doublet resulting from asymmetric division or of two polarized cells resulting from a symmetric division (green, Pearson R = -0.011, n = 3 symmetric doublets, $p > 0.1$), from 4 experiments. The rates are correlated, which suggests that the dynamics of internalization and the dynamics of building up of cortical asymmetries are linked.

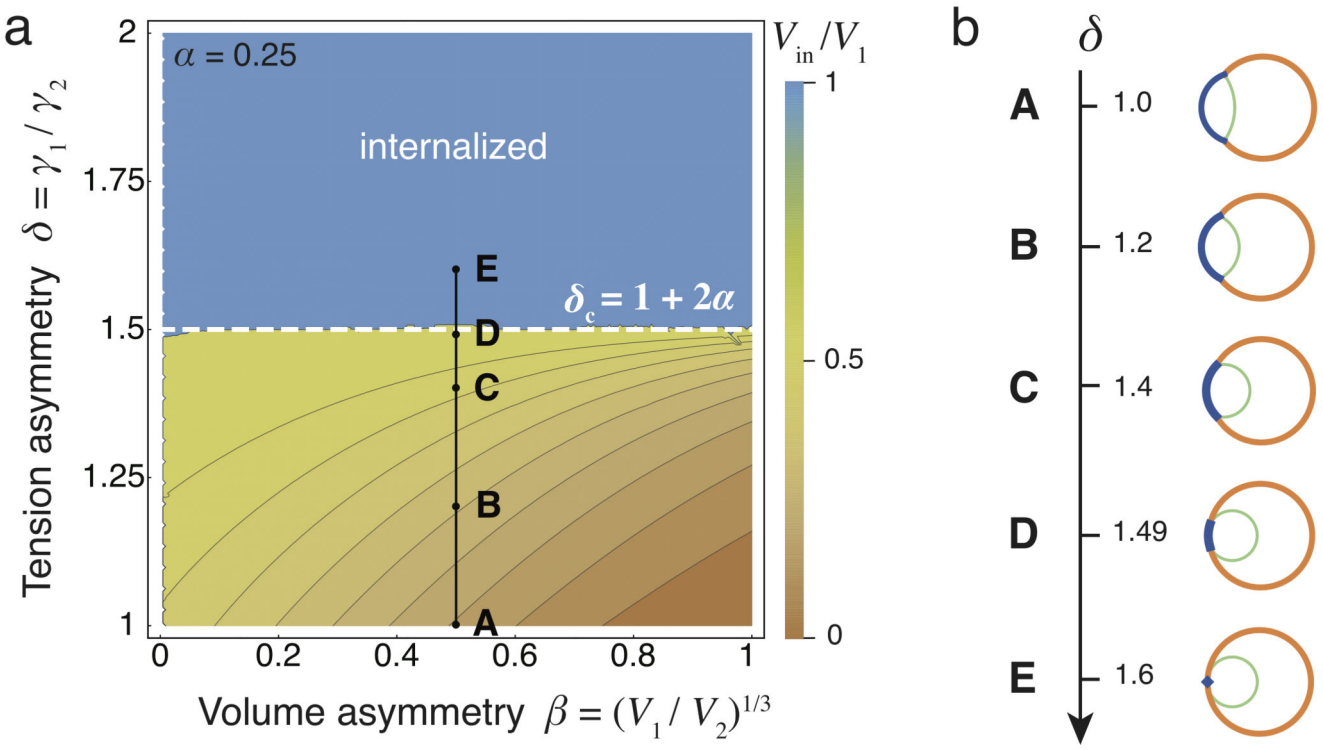

Extended Data Figure 3. Cell size has no influence on internalization

(a) Phase diagram describing the mechanical equilibrium of a cell within a doublet or embryo as function of the cell size asymmetry parameter β and the tension asymmetry parameter δ, for a fixed compaction parameter $\alpha = 0.25$. The color code measures the degree of internalization, defined as the proportion of internalized volume V_{in}/V_1, which equals 1 for the internalized cell. The dotted line indicates the threshold value δ_c at which

internalization occurs. An example of internalization with $\beta = 0.5$ is indicated in black (from A to E). Changing the volume asymmetry does not change the internalization threshold. (b) Internalization of a doublet with $\beta = 0.5$ obtained with the analytical model for the same values of δ as indicated in the diagram from A to E.

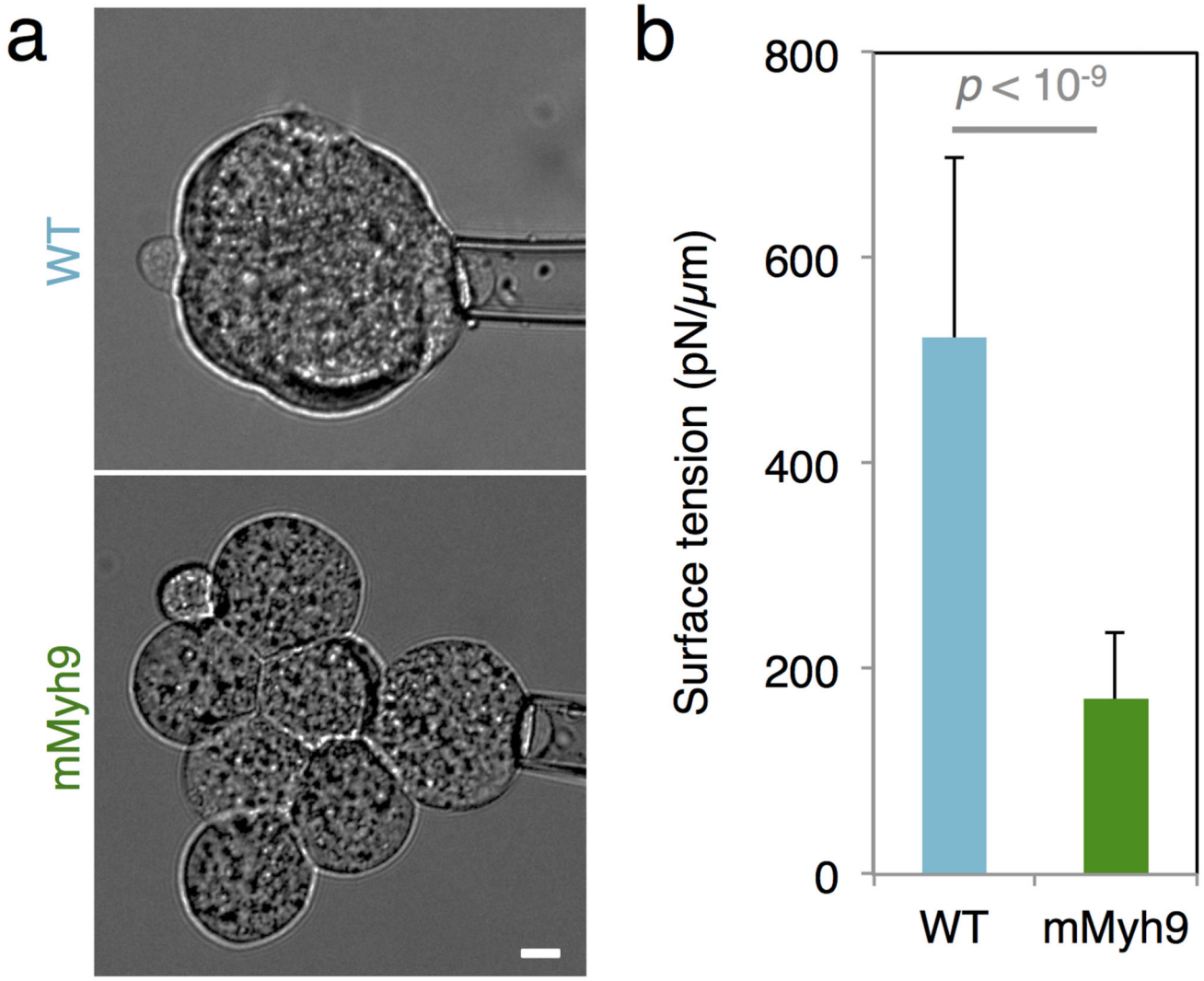

Extended Data Figure 4. Contractility is required for internalization

(a) Brightfield images of tension measurement on WT (top) and mMyh9 (bottom) 8-cell stage embryos. Scale bar 10 μm.

(b) Mean ± SD of 25 blastomeres from 4 WT embryos and 26 blastomeres from 7 mMyh9 embryos from 2 experiments, Student *t* test $p < 10^{-9}$.

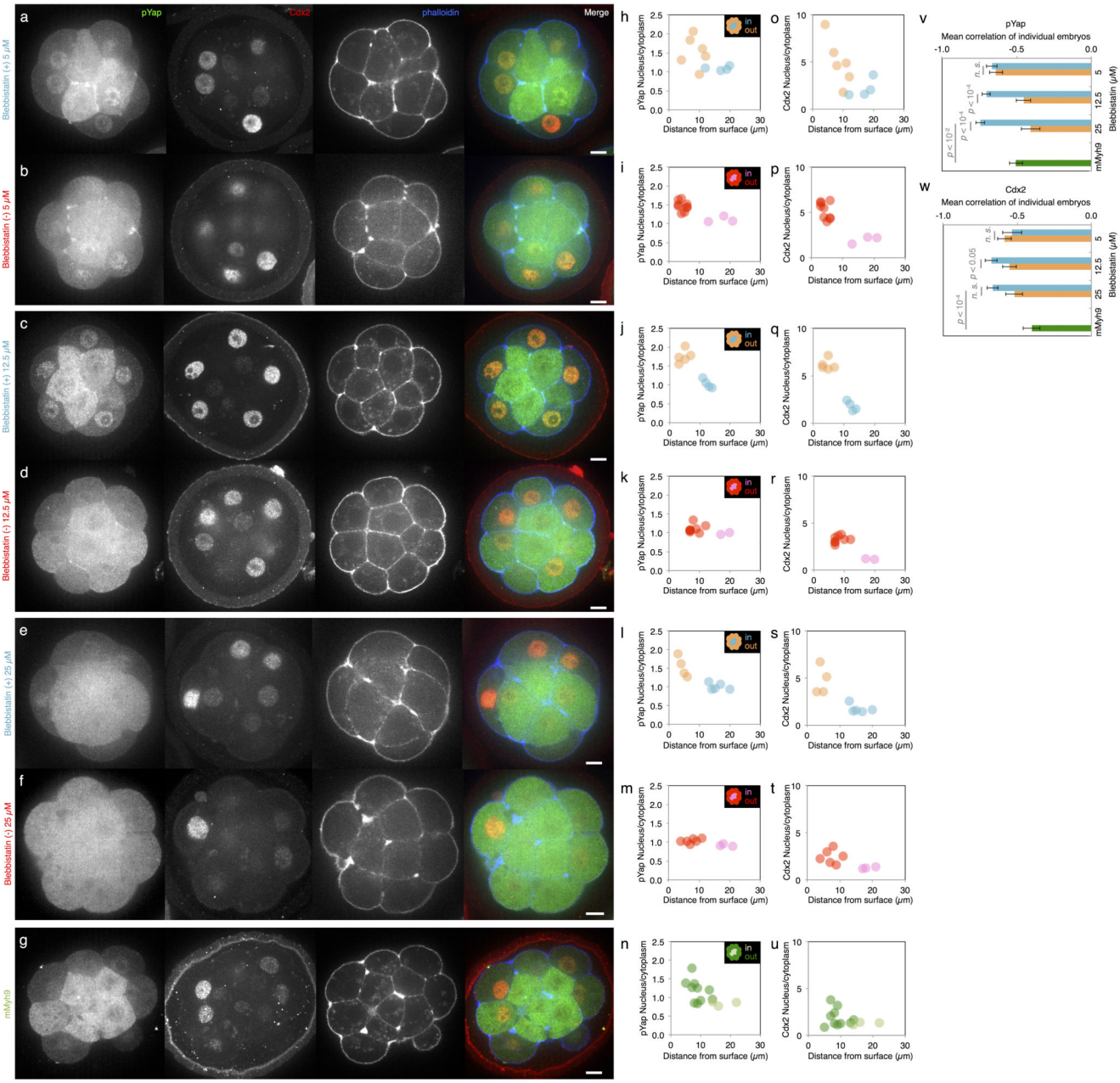

Extended Data Figure 5. Control of pYap and Cdx2 localization by contractility in a dose dependent manner

(a-g) Immunostaining of wild-type embryos treated for 3 h with Bb(+) at 5 (a), 12.5 (c) or 25 (e) μM or with Bb(-) at 5 (b), 12.5 (d) or 25 (f) μM or of mMyh9 embryos (g) showing phosphorylated Yap (pYap, green), Cdx2 (red) and phalloidin (blue).

(h-u) Nucleus to cytoplasm intensity ratio of pYap (h-n) or Cdx2 (o-u) as a function of the distance from the surface for WT embryo treated with Bb(+) (outer cells in orange and inner cells in blue) at 5 (h, o, corresponding embryo shown in a), 12.5 (j, q, corresponding embryo shown in c) or 25 (l, s, corresponding embryo shown in e) μM or with Bb(-) (outer cells in red and inner cells in pink) at 5 (i, p, corresponding embryo shown in b), 12.5 (k, r,

Europe PMC Funders Author Manuscripts

corresponding embryo shown in d) or 25 (m t, corresponding embryo shown in f) μM and for mMyh9 embryos (n, u, corresponding embryo shown in g).
(v-w) Mean ± SEM Pearson correlation values between the nucleus to cytoplasm intensity ratio of pYap (v) or Cdx2 (w) as a function of the distance from the surface from individual embryos. 207 blastomeres from 20 embryos for Bb(+) 5 μM, 252 blastomeres from 29 embryos for Bb(+) 12.5 μM, 179 blastomeres from 18 embryos for Bb(-) 5 μM and 267 blastomeres from 28 embryos for Bb(-) 12.5 μM from 3 experiments each. 281 cells from 28 embryos from 5 experiments for pYap and 136 cells from 13 embryos from 4 experiments for Cdx2 for 25 μM Bb(+), 241 cells from 32 embryos from 5 experiments for pYap and 192 cells from 22 embryos from 4 experiments for Cdx2 for 25 μM Bb(-) and 349 cells from 32 embryos from 6 experiments for pYap and 217 cells from 21 embryos from 3 experiments for Cdx2 for mMyh9. Student *t* test *p* values, *n. s.* for not significant.

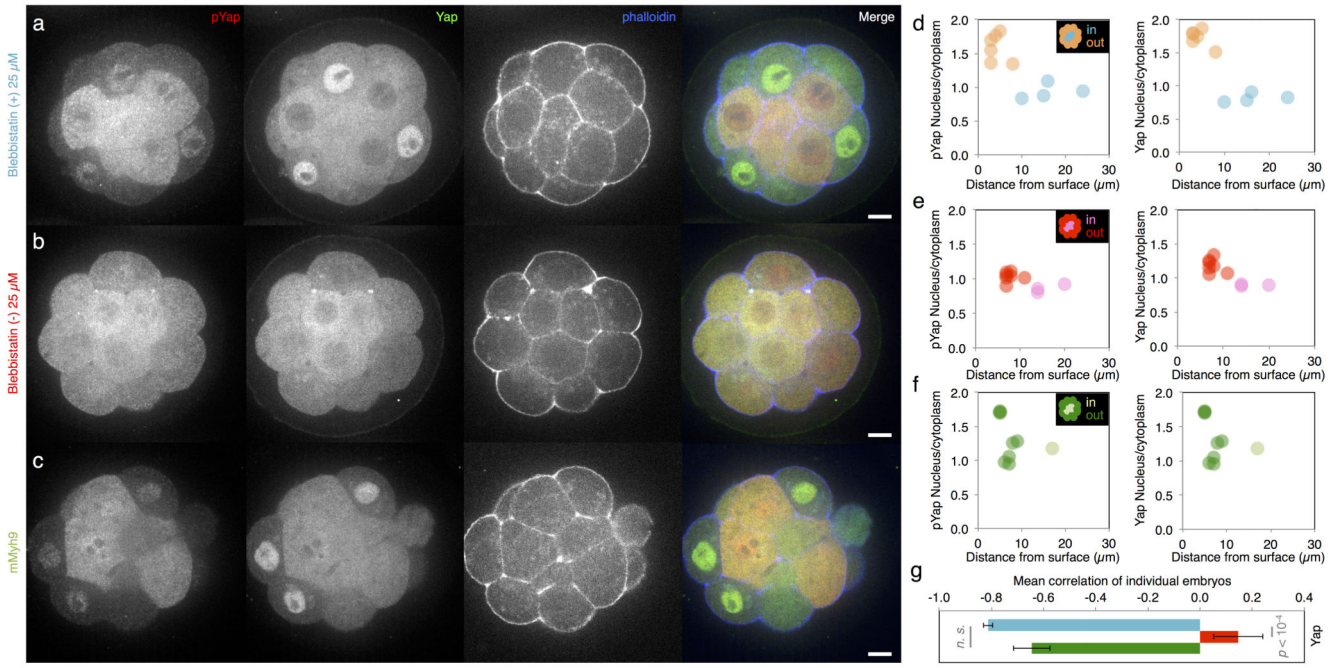

Extended Data Figure 6. Contractility controls Yap sub-cellular localization
(a-c) Immunostaining of wild-type embryos treated with 25 μM Bb(+) (a, an inactive enantiomere of the inhibitor) or Bb(-) (b, the selective inhibitor of myosin II ATPase activity) for 3 h or mMyh9 embryos (c) showing Yap (green), phosphorylated Yap (pYap, red) and phalloidin (blue).
(d-f) Nucleus to cytoplasm intensity ratio of pYap (left) and Yap (right) as a function of the distance from the surface for WT embryo treated with 25 μM Bb(+) (d, outer cells in orange and inner cells in blue, corresponding embryo shown in a) or Bb(-) (e, outer cells in magenta and inner cells in red, corresponding embryo shown in b) or mMyh9 embryo (f, outer cells in dark green and inner cells in light green, corresponding embryo shown in c).
(g) Mean ± SEM Pearson correlation values between the nucleus to cytoplasm intensity ratio of Yap as a function of the distance from the surface from individual embryos. 252 cells from 29 embryos for Bb(+), 201 cells from 26 embryos for Bb(-) and 132 cells from 12

embryos for mMyh9 from 3 experiments each. Student *t* test *p* value is shown, *n. s.* for not significant.

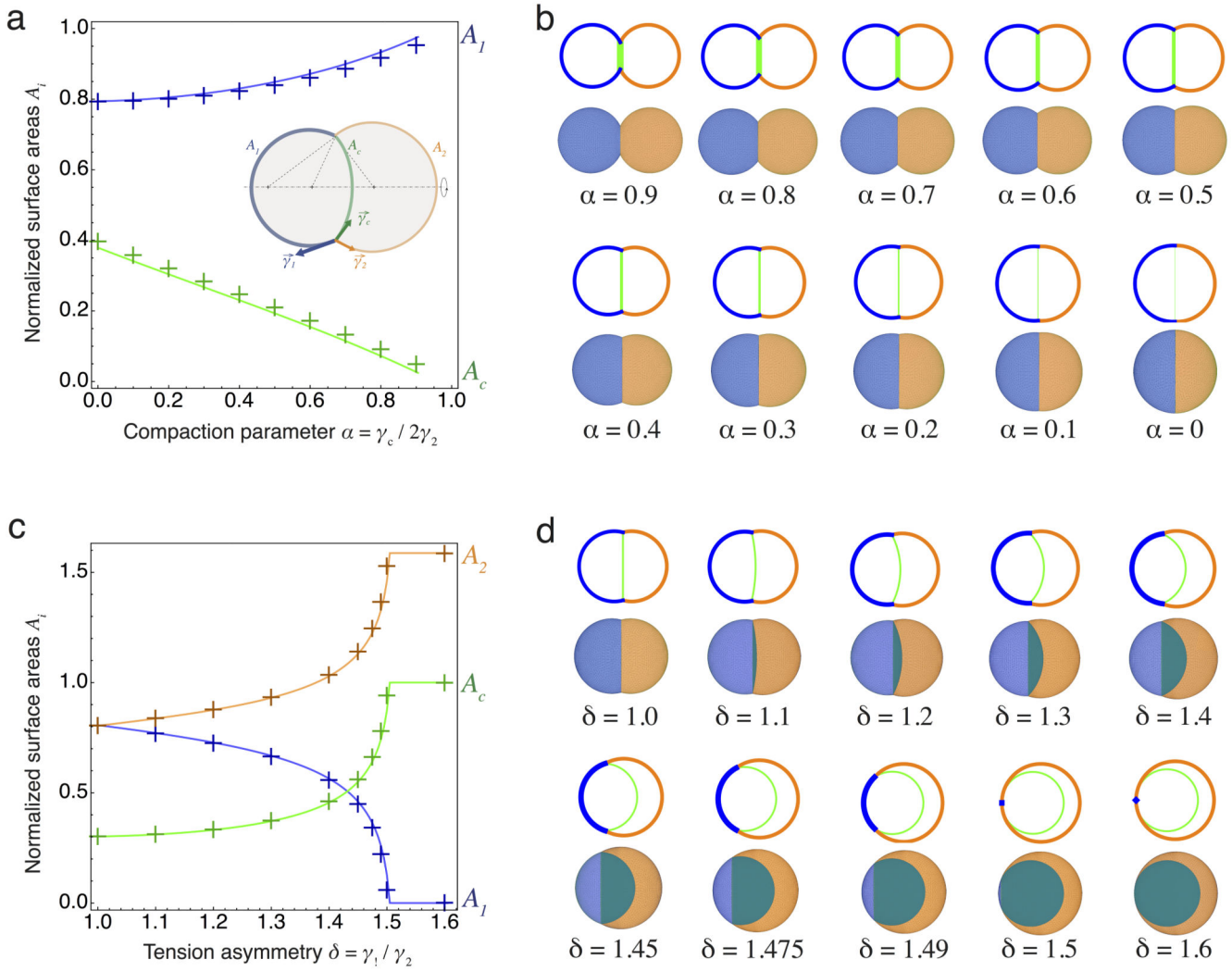

Extended Data Figure 7. Quantitative comparison between analytical and numerical results

(a) Comparison of the surface areas of the cell-medium (blue) and cell-cell interfaces (green) between the simulations (crosses) and the analytical model (plain lines) for different values of the compaction parameter α between 0 and 1. A schematic diagram of a cell doublet defining the cell-medium and cell-cell surface tensions γ_1, γ_2 and γ_c and areas A_1, A_2 and A_c are shown as an inset.

(b) Configurations of doublets as predicted by the analytical model and simulations for the discrete values of α corresponding to the plot in (a).

(c) Comparison of the surface areas of the cell-medium interfaces of cell 1 (blue), 2 (orange) and of the cell-cell interface (green) between the simulations (crosses) and the analytical model (plain lines) for different values of the tension asymmetry parameter δ between 1 and 1.6 t fixed compaction parameter α = 0.25.

Europe PMC Funders Author Manuscripts

(d) Configurations of doublets as predicted by the analytical model and simulations for the discrete values of δ corresponding to the plot in (b).

Supplementary Material

Refer to Web version on PubMed Central for supplementary material.

Acknowledgements

We are grateful to the Hiiragi lab members and EMBL animal facility for their support. We thank F. Da and C. Batty for helpful discussions on the simulations. We thank Y. Bellaïche for comments on an earlier version of the manuscript. Marie Curie individual fellowships under FP7 and H2020 programs support J-L.M., H.T. and R.N. under REA grant agreements n° 329044, 656306 and 326701 respectively. H.T. acknowledges support from the Bettencourt-Schueller and Joachim Herz foundations. The Hiiragi laboratory is supported by EMBL, ERC and VolkswagenStifftung.

References

1. Wennekamp S, Mesecke S, Nédélec F, Hiiragi T. A self-organization framework for symmetry breaking in the mammalian embryo. Nat Rev Mol Cell Biol. 2013; 14:454–461.
2. Anani S, Bhat S, Honma-Yamanaka N, Krawchuk D, Yamanaka Y. Initiation of Hippo signaling is linked to polarity rather than to cell position in the pre-implantation mouse embryo. Development. 2014; 141:2813–2824. [PubMed: 24948601]
3. Samarage CR, et al. Cortical Tension Allocates the First Inner Cells of the Mammalian Embryo. Dev Cell. 2015; 34:435–447. [PubMed: 26279486]
4. Hirate Y, et al. Polarity-Dependent Distribution of Angiomotin Localizes Hippo Signaling in Preimplantation Embryos. Curr Biol. 2013; 23:1181–1194. [PubMed: 23791731]
5. Dard N, Louvet-Vallée S, Maro B. Orientation of mitotic spindles during the 8- to 16-cell stage transition in mouse embryos. PLoS ONE. 2009; 4:e8171. [PubMed: 19997595]
6. Dupont S, et al. Role of YAP/TAZ in mechanotransduction. Nature. 2011; 474:179–183. [PubMed: 21654799]
7. Johnson MH. From mouse egg to mouse embryo: polarities, axes, and tissues. Annu Rev Cell Dev Biol. 2009; 25:483–512. [PubMed: 19575654]
8. Watanabe T, Biggins JS, Tannan NB, Srinivas S. Limited predictive value of blastomere angle of division in trophectoderm and inner cell mass specification. Development. 2014; 141:2279–2288. [PubMed: 24866117]
9. Johnson MH, Ziomek CA. The foundation of two distinct cell lineages within the mouse morula. Cell. 1981; 24:71–80. [PubMed: 7237545]
10. Matsumoto M, et al. PKClambda in liver mediates insulin-induced SREBP-1c expression and determines both hepatic lipid content and overall insulin sensitivity. J Clin Invest. 2003; 112:935–944. [PubMed: 12975478]
11. Hirate Y, et al. Par-aPKC-dependent and -independent mechanisms cooperatively control cell polarity, Hippo signaling, and cell positioning in 16-cell stage mouse embryos. Dev Growth Differ. 2015; 57:544–556. [PubMed: 26450797]
12. Maître J-L, Niwayama R, Turlier H, Nédélec F, Hiiragi T. Pulsatile cell-autonomous contractility drives compaction in the mouse embryo. Nat Cell Biol. 2015; 17:849–855. [PubMed: 26075357]
13. Lehtonen E. Changes in cell dimensions and intercellular contacts during cleavage-stage cell cycles in mouse embryonic cells. J Embryol Exp Morphol. 1980; 58:231–249. [PubMed: 7441156]
14. Heisenberg C-P, Bellaïche Y. Forces in tissue morphogenesis and patterning. Cell. 2013; 153:948–962. [PubMed: 23706734]
15. Overholtzer M, et al. A Nonapoptotic Cell Death Process, Entosis, that Occurs by Cell-in-Cell Invasion. Cell. 2007; 131:966–979. [PubMed: 18045538]
16. Dietrich J-E, Hiiragi T. Stochastic patterning in the mouse pre-implantation embryo. Development. 2007; 134:4219–4231. [PubMed: 17978007]

17. Johnson MH, Ziomek CA. Cell interactions influence the fate of mouse blastomeres undergoing the transition from the 16- to the 32-cell stage. Developmental Biology. 1983; 95:211–218. [PubMed: 6825925]
18. Graner F, Glazier J. Simulation of biological cell sorting using a two-dimensional extended Potts model. Phys Rev Lett. 1992; 69:2013–2016. [PubMed: 10046374]
19. Brodland G. The Differential Interfacial Tension Hypothesis (DITH): a comprehensive theory for the self-rearrangement of embryonic cells and tissues. J Biomech Eng. 2002; 124:188–197. [PubMed: 12002128]
20. Guzowski J, Korczyk PM, Jakiela S, Garstecki P. The structure and stability of multiple micro-droplets. Soft Matter. 2012; 8:7269–7278.
21. Da F, Batty C, Grinspun E. Multimaterial mesh-based surface tracking. ACM Trans Graph. 2014
22. Krieg M, et al. Tensile forces govern germ-layer organization in zebrafish. Nat Cell Biol. 2008; 10:429–436. [PubMed: 18364700]
23. Maître J-L, et al. Adhesion Functions in Cell Sorting by Mechanically Coupling the Cortices of Adhering Cells. Science. 2012; 338:253–256. [PubMed: 22923438]
24. Jacobelli J, et al. Confinement-optimized three-dimensional T cell amoeboid motility is modulated via myosin IIA-regulated adhesions. Nat Immunol. 2010; 11:953–961. [PubMed: 20835229]
25. Wang A, et al. Nonmuscle myosin II isoform and domain specificity during early mouse development. Proc Natl Acad Sci USA. 2010; 107:14645–14650. [PubMed: 20679233]
26. Aragona M, et al. A mechanical checkpoint controls multicellular growth through YAP/TAZ regulation by actin-processing factors. Cell. 2013; 154:1047–1059. [PubMed: 23954413]
27. Benham-Pyle BW, Pruitt BL, Nelson WJ. Cell adhesion. Mechanical strain induces E-cadherin-dependent Yap1 and β-catenin activation to drive cell cycle entry. Science. 2015; 348:1024–1027. [PubMed: 26023140]
28. Shin J-W, et al. Contractile forces sustain and polarize hematopoiesis from stem and progenitor cells. Cell Stem Cell. 2014; 14:81–93. [PubMed: 24268694]
29. Riedl J, et al. Lifeact mice for studying F-actin dynamics. Nature Methods. 2010; 7:168–169. [PubMed: 20195247]
30. Muzumdar MD, Tasic B, Miyamichi K, Li L, Luo L. A global double-fluorescent Cre reporter mouse. genesis. 2007; 45:593–605. [PubMed: 17868096]
31. Balbach ST, et al. Nuclear reprogramming: kinetics of cell cycle and metabolic progression as determinants of success. PLoS ONE. 2012; 7:e35322. [PubMed: 22530006]
32. de Vries WN, et al. Expression of Cre recombinase in mouse oocytes: a means to study maternal effect genes. genesis. 2000; 26:110–112. [PubMed: 10686600]
33. Ma X, et al. Conditional Ablation of Nonmuscle Myosin II-B Delineates Heart Defects in Adult Mice. Circulation Research. 2009; 105:1102–1109. [PubMed: 19815823]

Europe PMC Funders Author Manuscripts

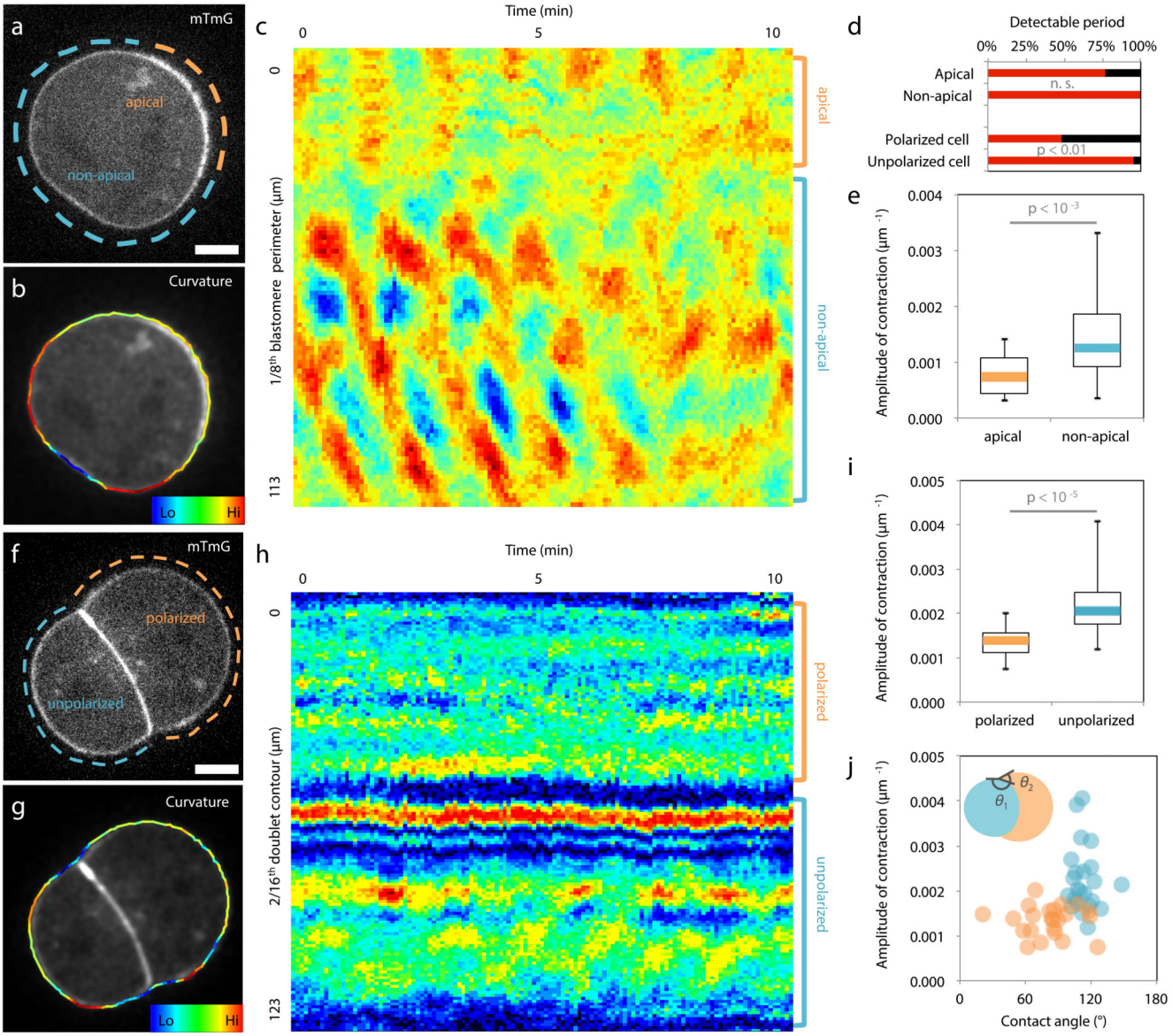

Figure 1. Asymmetric inheritance of the apical domain generates blastomeres of different contractility

(a-c) 8-cell stage blastomere expressing mTmG (a) with color-coded surface curvature (b) and corresponding kymograph (c). Apical domain highlighted in orange and non-apical cortex in blue.

(d) Proportion of blastomeres for which a contraction period can be detected (17 blastomeres and 23 doublets from 4 and 5 experiments respectively). Mann-Whitney *U* test *p* value, *n. s.* for not significant.

(e) Boxplot of contraction amplitudes for apical (orange) and non-apical cortex (blue). 17 blastomeres from 4 experiments, Student *t* test *p* value.

(f-h) Doublet of 16-cell stage blastomeres expressing mTmG (f) with color-coded surface curvature (g) and corresponding kymograph (h). Polarized blastomere highlighted in orange, unpolarized one in blue.

(i) Boxplot of contraction amplitudes for polarized (orange) and unpolarized blastomeres (blue). 23 doublets from 5 experiments, Student *t* test *p* value.
(j) Amplitude of contractions as a function of the contact angles θ_1 for polarized (orange) and θ_2 for unpolarized blastomeres (blue, Pearson R = -0.611, n = 46 blastomeres from 5 experiments, $p < 0.001$).
Scale bar 10 μm.

Europe PMC Funders Author Manuscripts

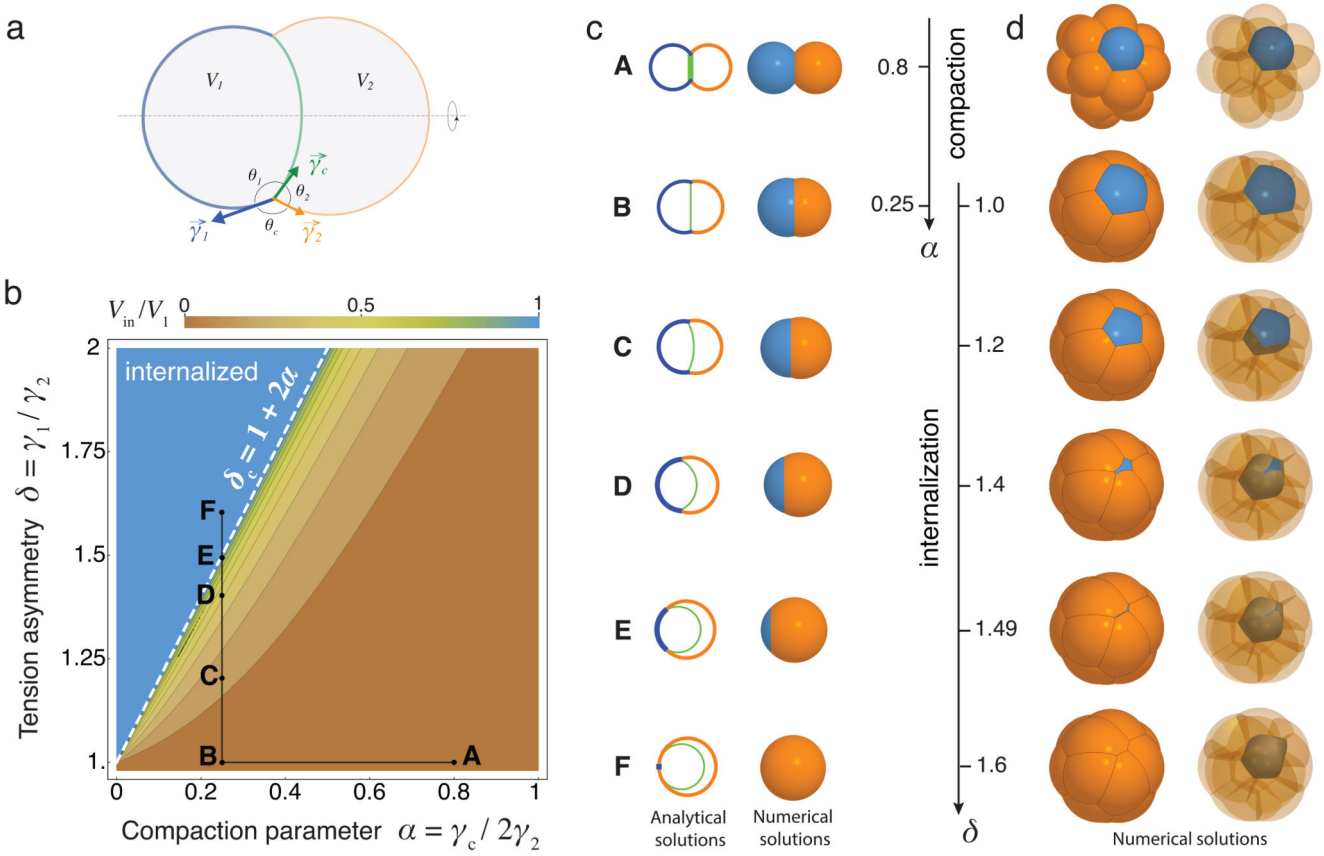

Figure 2. Physical model of cell internalization

(a) Schematic diagram of a cell doublet with surface tensions γ_1, γ_2 and γ_c of the cell 1 (blue), 2 (orange) and the contact (green) respectively. Contact angles θ_1, θ_2 and θ_c and cell volumes V_1 and V_2 are also shown.

(b) Phase diagram describing the mechanical equilibrium of a doublet as a function of the compaction parameter α and tension asymmetry δ. Color-coded degree of internalization (measured as the relative volume of cell 1 that is internalized V_{in}/V_1), threshold value δ_c at which internalization occurs (white dotted line) and an example of compaction (A to B) followed by internalization (B to F) in black (Supplementary Video 3-4) are overlaid.

(c-d) Analytical (left) and numerical solutions (right) for a doublet (c). Numerical solutions (d) for the compaction of 16 cells with opaque (left) and transparent (right) non-internalizing cells. The compaction parameter α decreases from 0.8 to 0.25, followed by an increase of tension asymmetry δ from 1.0 to 1.6.

Europe PMC Funders Author Manuscripts

Europe PMC Funders Author Manuscripts

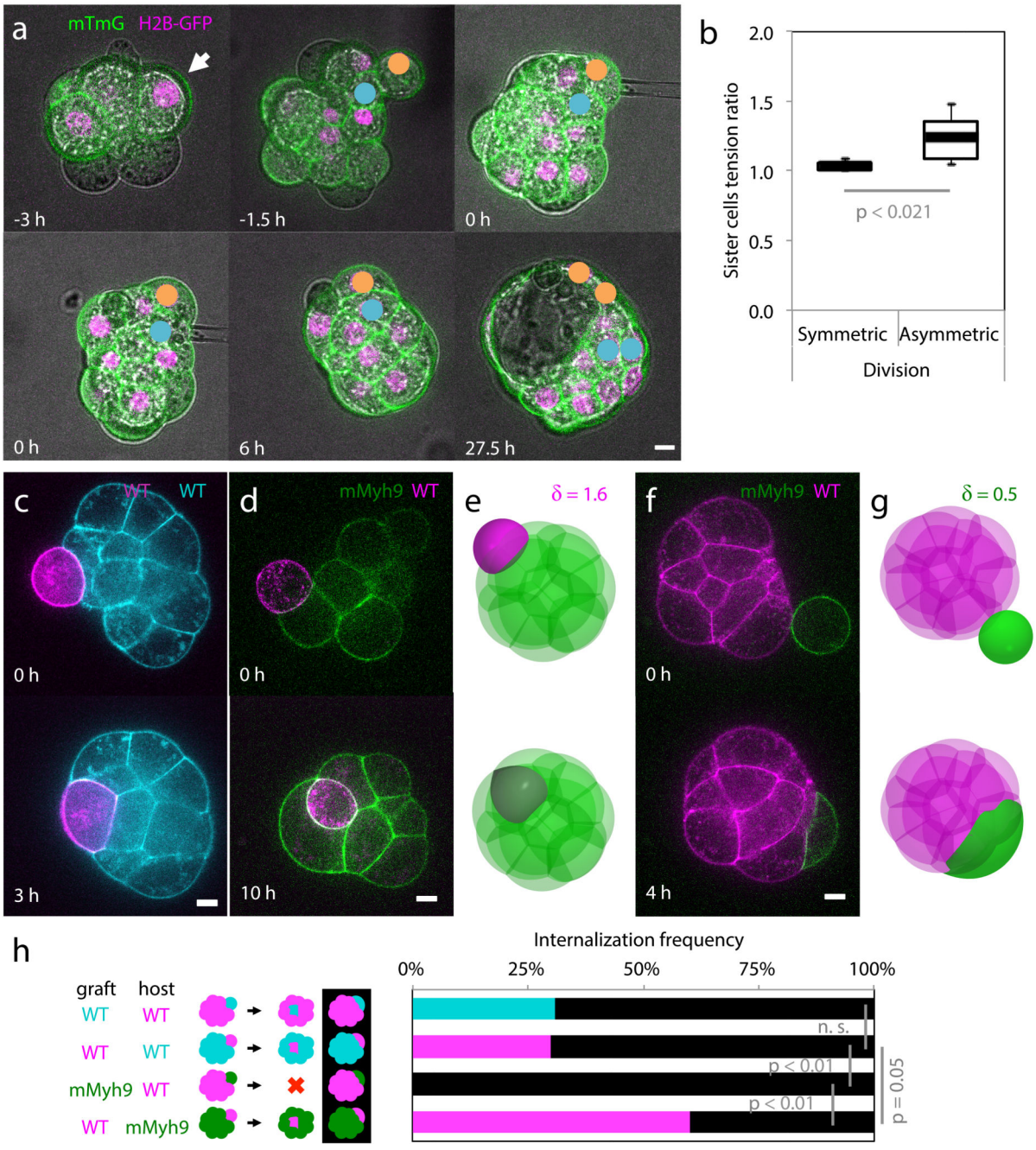

Figure 3. Tension heterogeneities drive cell sorting of the inner cell mass

(a) Lineage tracking of polarized (yellow) and unpolarized (blue) daughter cells after surface tension measurement of mTmG (green) H2B-GFP (magenta) expressing embryos.

(b) Box plot of surface tension ratio for sister cells with (symmetric) or without (asymmetric) internalization of one of the sister cell. 8 and 7 pairs of cells from 11 embryos from 5 experiments, Student *t* test *p* values.

(c-g) WT (magenta or cyan) or mMyh9 (green) blastomeres grafted onto host embryos (c, d, f). Simulations of grafting experiments: one cell with $\delta = 1.6$ (e), corresponding to WT onto mMyh9 (d); one cell with $\delta = 0.5$ (g), corresponding to mMyh9 onto WT (f).
(h) Internalization frequencies for chimeric embryos (WT-WT (13 mG host embryos and 20 mTmG host embryos from 3 experiments) and WT-mMyh9 (12 mG host embryos and 20 mMyh9 host embryos from 4 experiments)). Black when no internalization occurs, Mann-Whitney *U* test *p* values, *n. s.* for not significant.
Scale bar 10 μm.

Europe PMC Funders Author Manuscripts

Europe PMC Funders Author Manuscripts

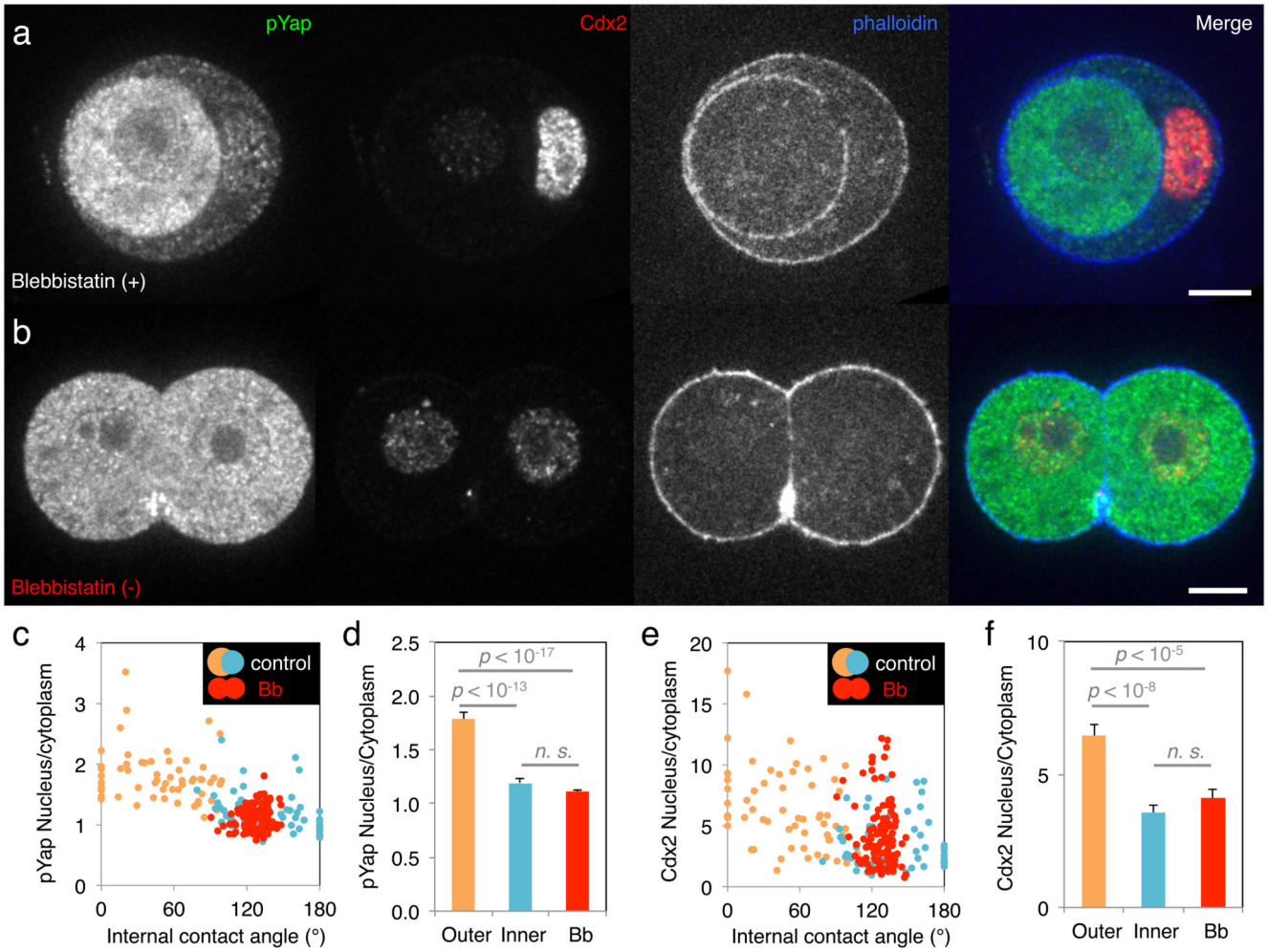

Figure 4. Contractility couples morphogenesis and fate specification

(a-b) Immunostaining of doublets of 16-cell stage blastomeres treated with 25 μM Blebbistatin (Bb) (+) (a, an inactive enantiomere of the inhibitor) or Bb(-) (b, the selective inhibitor of myosin II ATPase activity) showing pYap (green), Cdx2 (red) and phalloidin (blue).

(c-f) Nucleus to cytoplasm intensity ratio of pYap (c) or Cdx2 (e) as a function of the internal contact angle for doublets treated with Bb(+) (outer cells in orange and inner cells in blue, pYap R = -0.630, or Cdx2 R = -0.493, n = 59 doublets from 3 experiments, $p < 0.001$) or Bb(-) (red, pYap R = 0.158, or Cdx2 R = -0.118, n = 60 doublets from 3 experiments, $p > 0.1$). Mean ± SEM nucleus to cytoplasm intensity ratio of pYap (d) or Cdx2 (f). Doublets treated with Bb(+) show outer cells in orange, inner cells in blue while Bb(-) treated cells are in red. Student *t* test *p* values, *n. s.* for not significant.